

# We are IntechOpen, the world's leading publisher of Open Access books Built by scientists, for scientists

5,800

Open access books available

142,000

International authors and editors

180M

Downloads

Our authors are among the

154

Countries delivered to

TOP 1%

most cited scientists

12.2%

Contributors from top 500 universities



WEB OF SCIENCE™

Selection of our books indexed in the Book Citation Index  
in Web of Science™ Core Collection (BKCI)

Interested in publishing with us?  
Contact [book.department@intechopen.com](mailto:book.department@intechopen.com)

Numbers displayed above are based on latest data collected.  
For more information visit [www.intechopen.com](http://www.intechopen.com)



# Tunable Filter

*Di Lu*

## Abstract

Tunable filters enable dynamic spectrum access for the wireless systems, and the tunable bandpass filters with constant bandwidth (BW) are most favorable for practical applications. This chapter investigates the synthesis and realization techniques for the tunable filters using the coupling matrix with variable entries synthesizes the tunable filter and guides the filter design. The synthesis method and the matrix extraction procedures for the constant-bandwidth bandpass filter are included, and the typical numerical examples are given. This chapter also discusses the relationship between the theoretical matrix and the physical circuits, and then a planar tunable filter design is presented to verify this relationship. Furthermore, the general approach to designing the constant-bandwidth filters using the element variable coupling matrix is concluded. The planar circuit, as well as the 3D structure realizations, are offered to practically demonstrate the synthesis design approach.

**Keywords:** tunable filter, constant bandwidth, constant shape, synthesis of tunable filter, element variable coupling matrix

## 1. Introduction

The tunable filter is generally employed as a switched filter bank with a substantially reduced size. It self-adaptive selects the frequency spectrum and filters out undesired signals to meet the need for tunability/reconfiguration in wireless systems. As exemplified in **Figure 1**, the core part of a typical mobile transceiver module is realized by a transceiver IC with many blocks of filters (or multiplexers), switch matrices, power amplifiers, and two antennas. The filters and switch matrices constitute the unintegrable switched filter banks that are used to select the signal dynamically. It is predictable that if the compact and high-performance tunable filters replace the bulky filter banks, this part of the circuit will consist of only a transceiver IC, two tunable filters, a wideband power amplifier, and two antennas (right side of **Figure 1**). Nowadays, with a more complex wireless electromagnetic environment, the frequency spectrum is more crowded, and thus it is even more significant to facilitate efficient utilization of the available frequency spectrum. The tunable filter, which plays a crucial role in utilizing the frequency spectrum, has become the hotspot not only in the research area but also for industrial applications.

The filter with tunability and without too much Q degradation known as the high-Q tunable filter has been widely used in the industry. Magnetically tunable filters or yttrium iron garnet (YIG) filter, which provides the tunable band with the high Q factor and multi-octave tuning range, is the essential part in front-ends of the microwave test and

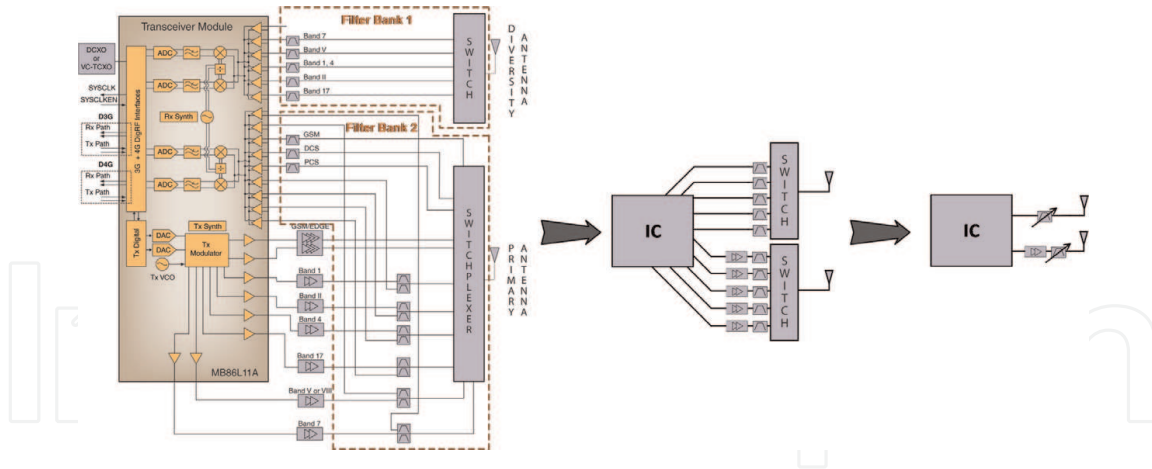


**Figure 1.** Tunable filters replace switched filter banks with a substantially reduced size [1].

measurement instruments [2, 3]. This type of filter can be tunable by magnetically adjusting the ferrimagnetic resonance of the crystal YIG spheres, thus resulting in the filter frequency adjustment. The mechanically tunable filter is another type of high-Q filter that can provide the high-Q tunable passband with a relatively compact size (compared with the YIG filter). This type of filter's frequency or response shape is reconfigured by changing the physical dimensions of the filter structures or disturbing the electromagnetic field in the resonators. The mechanically tunable filter has been commonly employed for tunable wireless infrastructure equipment or reconfigurable communication satellite operators to extend their service life and functionality [4–6]. A great deal of high-Q mechanically tunable filters, including coaxial, waveguide, or dielectric resonator structures, have been exploited. For example, mechanically adjusting the end-loading capacitors (or equivalent capacitors) of each coaxial resonator, the coaxial filter can be tunable with a wide tuning range [7–10]. The reconfigurability of the waveguide filter is enabled by reshaping the cavity dimension of the resonator or moving the perturbations inserted in the waveguide cavities [11–15]. For the dielectric resonator filter, moving the movable disks above the dielectric resonators can tune their resonant frequencies resulting in filter passband tunability [16–18].

The ever-increasing demand for the miniaturized and highly integrated wireless system requires the future tunable filter with a more compact size and fully electrical control. The giant tuning mechanisms inevitably make YIG filters and mechanically tunable filters oversize. With this regard, the electrically tunable filter with the semiconductor tuning element has been drawing a lot of attention and getting extensively exploited because of its very compact size, fast tuning speed, and straightforward control mechanism, even though the semiconductor tuning element loaded on the resonator will dramatically deteriorate the filter Q factor. Planar tunable filter is a popular research topic because of its easy integration with semiconductor tuning elements. For example, the planar  $\lambda/4$ ,  $\lambda/2$ , and multimode resonators loaded by tunable varactors or PIN diodes or both are employed to construct the tunable filters with frequency and bandwidth (BW) control [19–23]. In addition, emerging tuning semiconductor devices such as Radio Frequency Microelectromechanical Systems (RF-MEMS) and ferroelectric devices are also used as the variable capacitor in the planar tunable filters to alleviate the Q factor deterioration [20, 24–26]. Aside from the planar filter, the high-Q tunable three-dimensional (3D) filter with tuning semiconductor elements is also a research hotspot because of its low loss, good power handling, and high selectivity. For example, coaxial filters or quasi-coaxial

filters [7, 27–31], dielectric resonator filters [32, 33], and waveguide filters [34] are loaded by the various variable capacitors or switchable devices, thus constructing the tunable/reconfigurable 3D high-Q filters.

Among a large variety of tunable filters, the bandpass filter with the tunable center frequency (CF) is attractive for its widespread application. It is preferable to use the minimum number of tuning elements to control the frequency of the bandpass filter and realize the constant absolute bandwidth (BW). This realization will minimize the Q fact degradation introduced by the loaded tuning elements and maintain the filter response shape as the frequency is tuned. It is also the simplest tunable filter with the most straightforward control mechanism. Therefore, the tunable filter with constant bandwidth has been one of the emerging trends in filter design. For example, the planar filters [35–37], waveguide filters [15], coaxial filters [7], etc., have been all investigated to approach the constant-BW tunable filters.

In general, since the tunable filters have not large-scale replaced the filter banks, the research and development of the tunable filter is still indispensable, especially for the frequency tunable bandpass filter with constant bandwidth. This chapter will mainly deal with the tunable bandpass filter and offer the general synthesis-based approach. The synthesis method, tuning behavior, and physical realization techniques are included and discussed. The synthesis is based on the coupling matrix where the elements are variable, and the coupling matrix with the variable elements can represent the tunable filter response as well as the tuning behavior. The direct relationship between the matrix and the filter realization will be established, and thus various physical structures can be employed to realize the tunable filter accordingly. Furthermore, the constant-BW tunable filter will also be investigated, and the synthesis with its design approach will be included. A planar and a 3D tunable filter design examples will be offered to realize the theory.

## 2. Element variable coupling matrix (EVCM)

The coupling matrix is the most commonly used technique to synthesize the fixed filter. One can prescribe or optimize the filter function in terms of the fixed filter specification, and then the coupling matrix can be directly extracted from the filter function. After a few iterations of mathematical manipulation/optimization, the coupling matrix can physically correspond to the filter structures. This is the synthesis process for the fixed filter. However, for the tunable filter, the frequency of the resonator is variable. When the filter is tuning (tunable frequency or tunable BW), there are numerous filter prototypes (filter matrices) corresponding to the same filter response. As illustrated in **Figure 2**, one can extract three different coupling matrices according to the same filter response using different tuning frequencies ( $f_d$ ) and different tuning bandwidths (BWs). This means three coupling matrices can be corresponding to the same filter response. Obviously, the conventional coupling matrix is not appropriate to synthesize the tunable filter, and therefore the element variable coupling matrix (EVCM) is introduced.

The EVCM is derived from the conventional coupling matrix and can be treated as the tunable version of the coupling matrix. First of all, the conventional coupling matrix can be extracted using the frequency-fixed filter synthesis (e.g. using the matrix manipulation method [5] or optimization process [38]) based on the prescribed frequency response. For the lossless  $N \times N$  coupling matrix with the termination impedance  $R_1$ , the response is calculated based on the current loop model and voltage node model as:

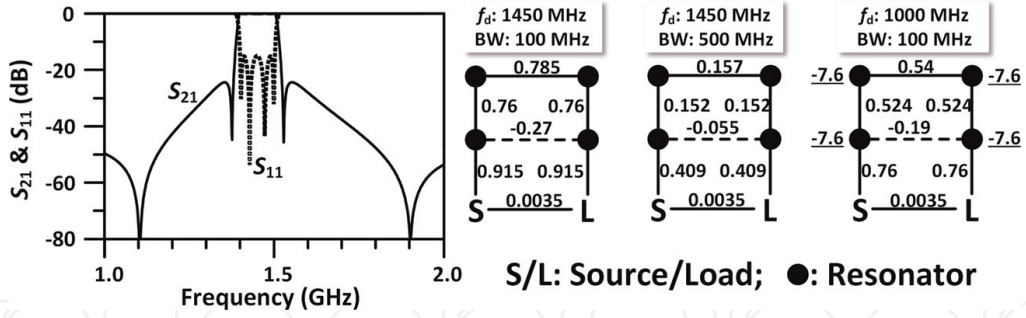


**Figure 2.**  
Same response of the three different classical coupling matrices.

$$\begin{cases} S_{21} = \frac{2R_1}{w_0L \times FBW_d} [A]^{-1}_{N,1} = \frac{2}{w_0CR_1 \times FBW_d} [A]^{-1}_{N,1} \\ S_{11} = 1 - \frac{2R_1}{w_0L \times FBW_d} [A]^{-1}_{1,1} = 1 - \frac{2}{w_0CR_1 \times FBW_d} [A]^{-1}_{1,1} \end{cases} \quad (1)$$

where

$$[A] = \begin{bmatrix} 1/(Q_e \times FBW_d) + \Lambda_d + jM_{11} & jM_{12} & \cdots & jM_{1n} \\ jM_{21} & \Lambda_d + jM_{22} & \cdots & jM_{2n} \\ \vdots & \vdots & \vdots & \vdots \\ jM_{n1} & jM_{n2} & \cdots & 1/(Q_e \times FBW_d) + \Lambda_d + jM_{kk} \end{bmatrix} \quad (2)$$

$$\begin{cases} \frac{1}{Q_e} = \frac{R_1}{w_0L} = \frac{1}{R_1w_0C} \\ \Lambda_d = j \left( \frac{f}{f_d} - \frac{f_d}{f} \right) / FBW_d \\ M_{kk} = \left( \frac{f_d}{f_{kk}} - \frac{f_{kk}}{f_d} \right) / FBW_d \end{cases} \quad (3)$$

$\Lambda_d$  and  $M_{ij}$  denote normalized frequency, and element of the coupling coefficient between resonator  $i$  and  $j$ .  $M_{kk}$  is the self-coupling coefficient or immittance, representing the corresponding resonator's frequency shift.  $f_{kk}$  is the resonant frequency of each resonator (or resonator  $k$ ). As implied by (1–3), the passband response is calculated from a coupling matrix when the CF (scaling frequency  $f_d$ ) and fractional bandwidth ( $FBW$ ) are given. However, for the tunable filter, both  $BW$  (or  $FBW$ ) and  $CF$  are variable. Thus, it is difficult to form a tunable passband by a coupling matrix and then realize the filter accordingly (as demonstrated in **Figure 2**). The tuning range and behavior are also important since the passband is tunable, but the conventional matrix cannot work. Therefore, the coupling matrix is reformulated as:

$$\begin{cases} S_{21} = \frac{2}{Q_e} [B]^{-1}_{N,1} \\ S_{11} = 1 - \frac{2}{Q_e} [B]^{-1}_{1,1} \end{cases} \quad (4)$$

$$[B] = \begin{bmatrix} 1 & & & \\ \frac{1}{Q_e + \lambda_d + jm_{11}} & jm_{12} & \cdots & jm_{1n} \\ jm_{21} & \lambda_d + jm_{22} & \cdots & jm_{2n} \\ \vdots & \vdots & \vdots & \vdots \\ jm_{n1} & jm_{n2} & \cdots & \frac{1}{Q_e + \lambda_d + jm_{kk}} \end{bmatrix} = ([Q_e] + \lambda_d[W] + j[m_\Delta]) \quad (5)$$

$$\begin{cases} \lambda_d = j \left( \frac{f}{f_d} - \frac{f_d}{f} \right) \\ m_{kk} = \left( \frac{f_d}{f_{kk}} - \frac{f_{kk}}{f_d} \right) \end{cases} \quad (6)$$

$$[Q_e] = \begin{bmatrix} \frac{1}{Q_e} & 0 & \cdots & 0 \\ 0 & 0 & \cdots & 0 \\ \vdots & \vdots & \vdots & \vdots \\ 0 & 0 & \cdots & \frac{1}{Q_e} \end{bmatrix} \quad (7)$$

Here, the denormalized matrix  $[m_\Delta]$  has an interesting feature. For demonstration, a dual-mode resonator filter (or two-order transversal filter) is taken as an example (as shown in **Figure 3**). The matrix  $[m_\Delta]$  of this filter can be extracted according to the aforementioned techniques as:

$$[m_\Delta] = \begin{bmatrix} m_{ee} & m_{eo} \\ m_{oe} & m_{oo} \end{bmatrix} = \begin{bmatrix} x & 0 \\ 0 & y \end{bmatrix} \quad (8)$$

For simplification, the external Q factors  $Q_{exe/exo}$  for two resonant modes are roughly approximate to  $Q_e$  as:

$$Q_e = \frac{(Q_{exe} + Q_{exo})}{2} \quad (9)$$

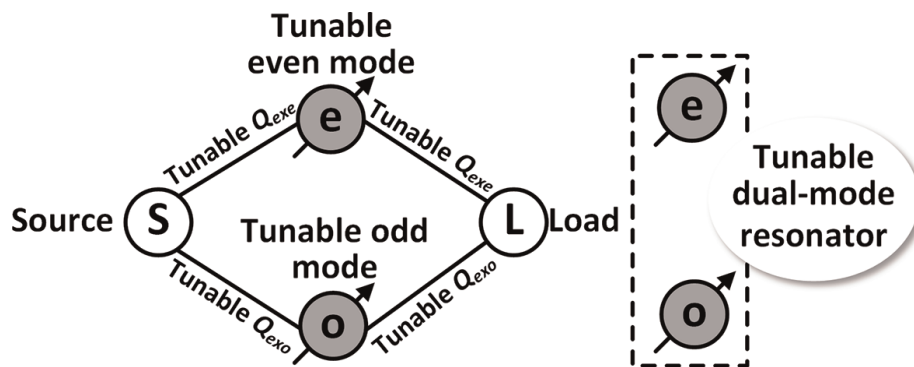


**Figure 3.** Architecture of the dual-mode resonator tunable filter.

It can be derived that

$$\begin{cases} x = f_d/f_e - f_e/f_d \\ y = f_d/f_o - f_o/f_d \\ Q_{exe/exo} = \frac{f_{exe/exo}}{\Delta f_{\pm 90}} \approx \frac{1}{FBW_{exe/exo}} = \frac{f_{exe/exo}}{BW_{exe/exo}} \end{cases} \quad (10)$$

Now, it can be found that all elements of matrix  $[m_{\Delta}]$  are directly related to the architecture. As long as the parameters of the architecture are defined with the given tuning ranges and the scaling frequency  $f_d$ , the responses of the tunable filter (e.g. tuning ranges of CF, BW, return loss (RL)) can be completely determined. The second-order filter example is given for demonstration, as shown in **Figure 4**, where the matrix is denoted as  $x, y$ , and  $Q_e$ . **Figure 5** presents the responses of the matrix when the  $x$  is varied. It is observed that only the even-mode resonant frequency is tuned, implying even-mode resonant frequency is independently controlled by  $x$ . Similarly, **Figures 6** and **7** show that the odd-mode frequency and RL independently varied by changing  $y$  and  $Q_e$ , which suggests that the odd-mode resonant frequency and the RL are independently controlled by  $y$  and  $Q_e$ .

With this interesting feature, a one-to-one correspondence between the tunable filter responses and this matrix can be established. As a result, the matrix can uniquely represent tunable filter responses. **Figures 8–10** presents the typical responses by purposely varying the matrix elements  $[m_{\Delta}]$ . As shown in **Figure 8**, the matrix elements  $x, y$ , and  $Q_e$  are changed from 0.058, 0.034, and 18.765 to 0.028, 0.044, and 27.777, thus forming a 0.8 GHz to 1.2 GHz CF-tunable filter response with a constant 130 MHz BW. Hence, this tunable filter can be synthesized by such a coupling matrix

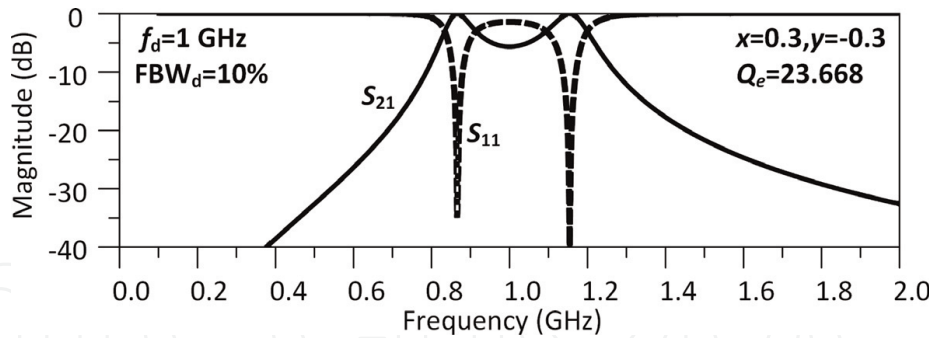


**Figure 4.**  
Theoretical response of a fixed filter example.

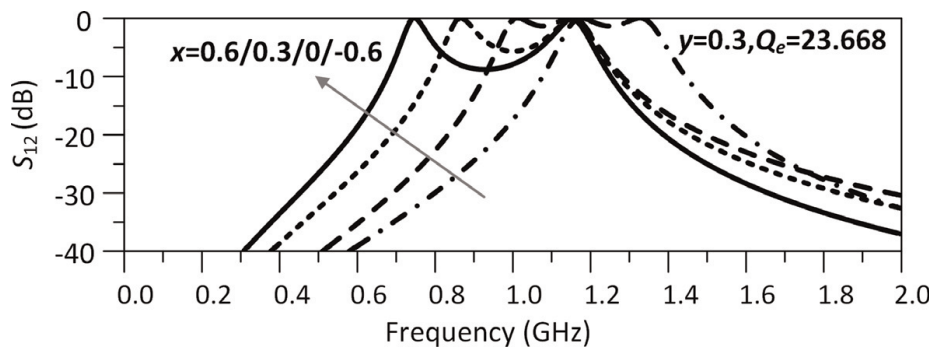


**Figure 5.**  
Theoretical curves for varying  $x$ .

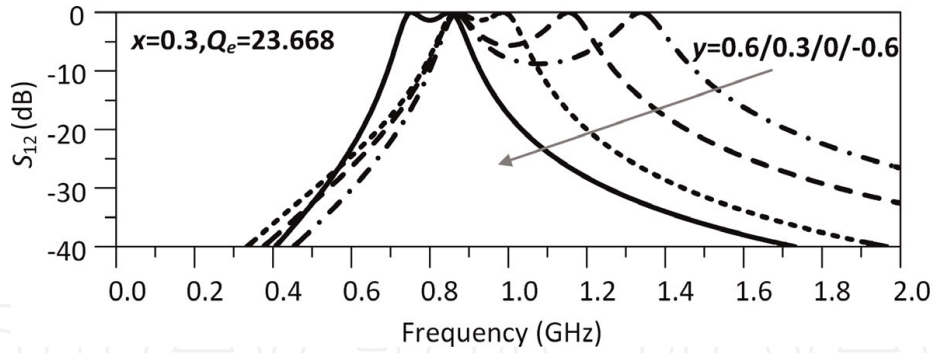


**Figure 6.**  
Theoretical curves for varying  $y$ .

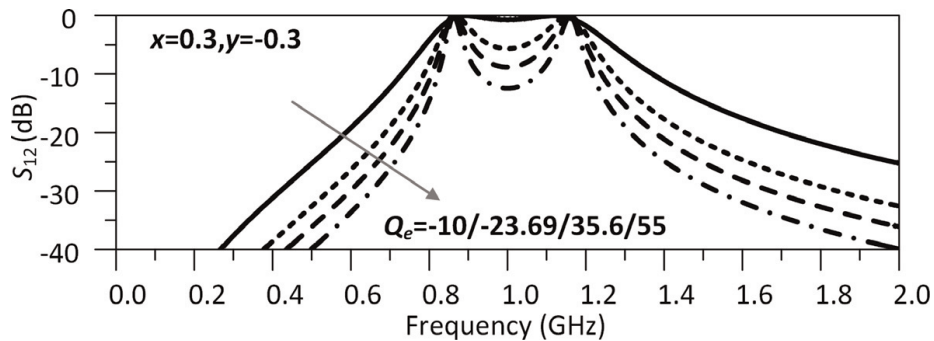


**Figure 7.**  
Theoretical curves for varying  $Q_e$ .

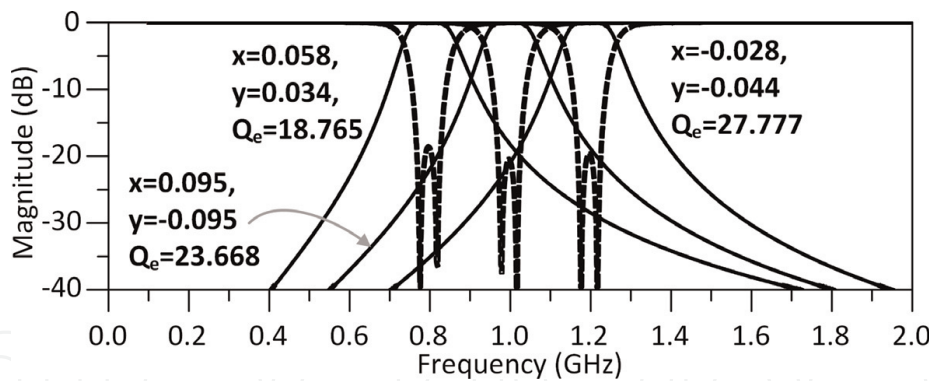


**Figure 8.**  
Theoretical curves for tuning the CF with 130-MHz 3-dB BW and 20-dB RL.

with these variable elements. Similarly, 130 MHz to 300 MHz BW-tunable filter responses with the constant 1 GHz CF (as shown in **Figure 9**) and RL-tunable filter responses with 1 GHz CF and 130 MHz BW (as shown in **Figure 10**) are formed by specifying the elements of the matrix. So, the element variable coupling matrix (EVCM) can synthesize these tunable filters.

The physical structure is presented to realize the EVCM, as shown in **Figure 11**. The given circuit is controlled by loaded varactor diodes, and each control element can be used to tune the entry of the EVCM separately. For example, the variable capacitor  $C_o$  and  $C_e$ , respectively, control the odd-mode and even-mode resonant frequencies, and adjusting  $C_m$  will tune the external quality factor  $Q_e$ . Therefore, this structure is a fully tunable filter. Since the multimode structures are challenging to be coupled with equal energy ( $Q_{exo} = Q_{exe}$ ) for every resonant mode, the added circuit configuration



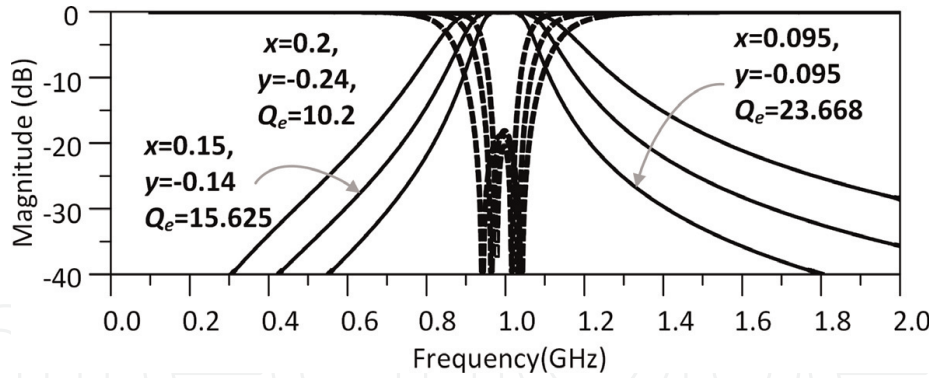


**Figure 9.**  
Theoretical curves for tuning the BW with 1 GHz CF and 20-dB RL.

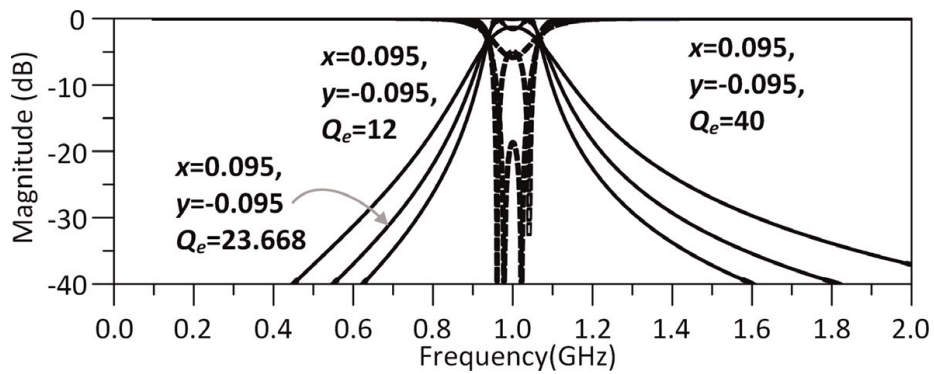


**Figure 10**  
Theoretical curves for the RL reconfiguration with 1 GHz CF and 130 MHz  $BW_{3db}$ .

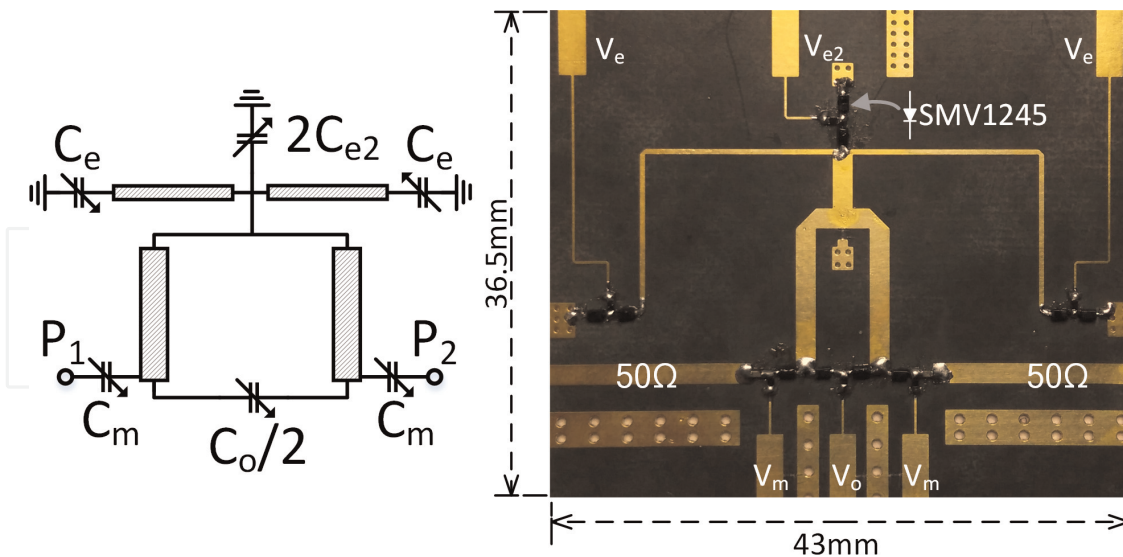


**Figure 11.**  
Transmission line model and physical circuit.

with  $C_{e2}$  is employed. Properly adjusting  $C_{e2}$  will enforce  $Q_{exo} = Q_{exe}$  and fully implement the EVCM.

Figures 12–14 presents the measurement results of the physical circuit corresponding to the calculated results of EVCM. As can be seen, the in-band responses of the filter are all very close to the given EVCM. The CF frequency of the filter can be tuned from 0.8 GHz to 1.2 GHz, and a 130-MHz 3-dB BW is kept nearly

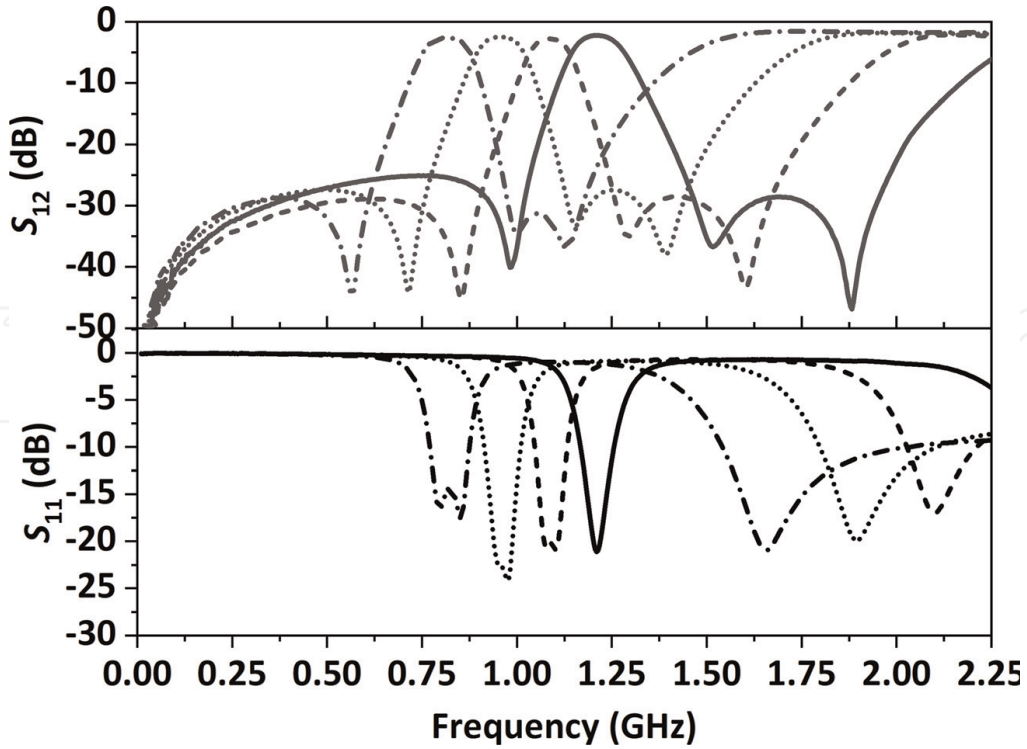


**Figure 12.**  
Measurement curves for tuning the CF with constant BW.

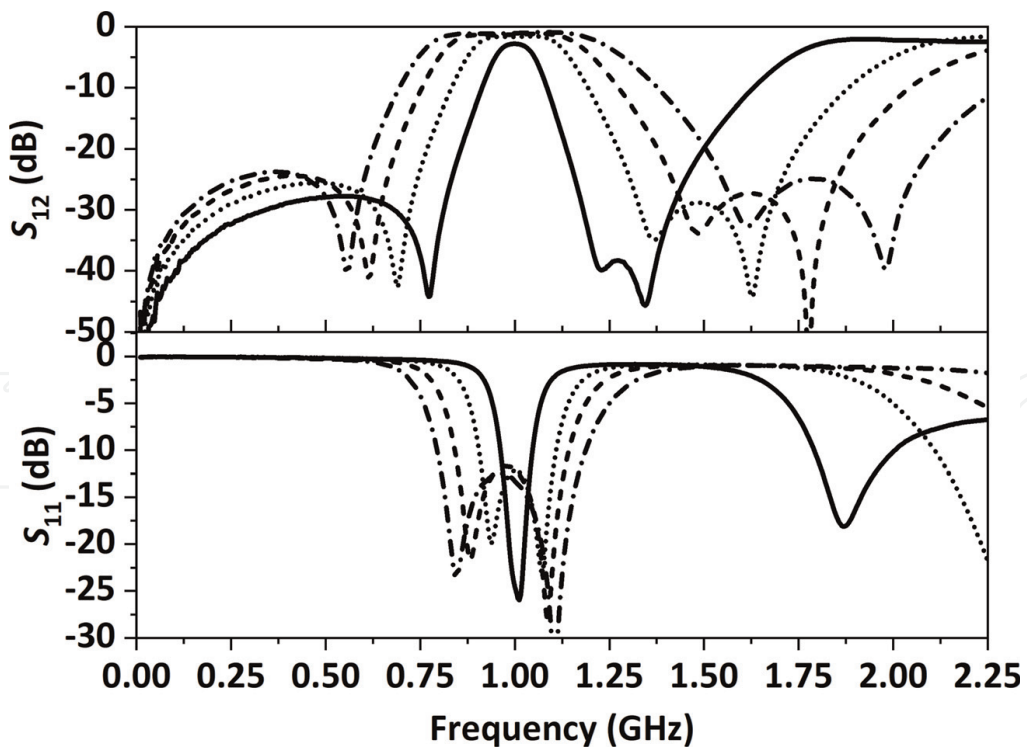


**Figure 13.**  
Measurement curves for tuning the BW with constant CF.

constant, as implied in **Figure 12**. These responses closely agree with the EVCM results as shown in **Figure 8**. The BW varying from 50 to 400 MHz is measured as shown in **Figure 13** when the circuit is fully tuned, which corresponds to the EVCM results as

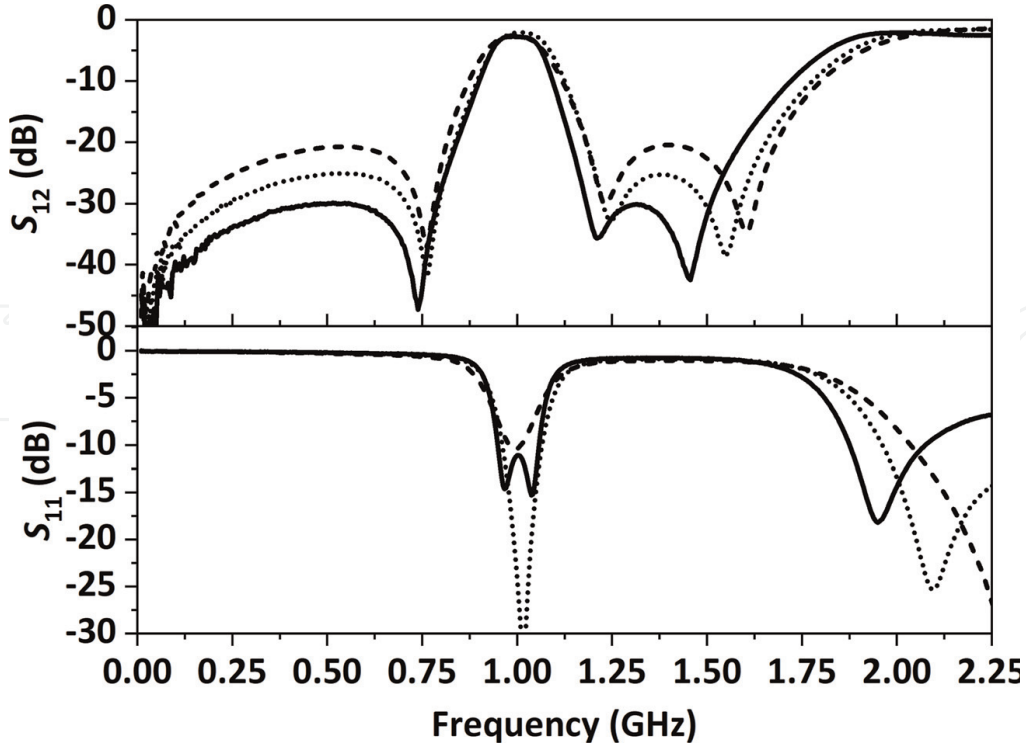


**Figure 14.**  
Measurement curves for tuning the RL with constant CF and BW.

shown in **Figure 9**. **Figure 14** shows the RL reconfiguration results of the filter. As shown, the passband is fixed at 1 GHz with 130-MHz BW, while the RL is reconfigured as prescribed by the EVCN (**Figure 10**) and the rejection is reshaped. The agreement between the experimental circuit and EVCN is obtained. Note that the practical circuit generates the transmission zeros to enforce  $Q_{exo} = Q_{exe}$ , which causes the major disagreement in the stopband. These three transmission zeros are owing to the added circuit configuration, which introduces an out-band resonant mode that forms one more coupling path from source to load and generates transmission zeros there.

### 3. Synthesis of the constant-BW filter using EVCN

With the introduction of the new matrix, the tunable filter can correspond to an EVCN uniquely. Thus, the tunable filter with constant BW can be synthesized with a few steps of the mathematical manipulations. First, for a tunable resonator, the adjustment of the CF is realized by tuning the loading effect, which can be treated as adding or subtracting the susceptance from the resonator. Thus, the tunable parameter of a resonator can be modeled by the corresponding diagonal element of an EVCN as:

$$m_{tt} = \left( \frac{f_d}{f_t} - \frac{f_t}{f_d} \right) \quad (11)$$

For the tunable coupled-resonator filters, it is reasonable to define  $m_{tt1} = m_{tt2} = m_{tt3} = \dots = m_{tt}$ , and thus, when the filter is adjusted, the frequencies of all the resonators will be tuned with the same tuning step. Additionally, to maintain the constant BW over a wide tuning range, when adjusting CF, the entries of the EVCN

(including the external quality factor  $Q_e$ ) are required to change in a specific manner synchronously.

Based on the earlier discussion, one may assume that the EVCMs are the linear functions of the variable  $m_{tt}$ , and thus the EVCN  $[m_{\Delta}]_t$  is converted as (12, 13).  $[m_{\Delta}]$  is the frequency-fixed part of the EVCN, which is unchanged when the frequency is tuned.  $[c]$  is a factor matrix and determines the passband variation rate of the filter. When tuning CF, the total matrix varies as predefined by  $[c]$ , which results in a tunable passband that varies in a linear function according to the predefined response and BW variation:

$$[m_{\Delta}]_t = \begin{bmatrix} m_{11} + c_{11}m_{tt} & m_{12} + c_{12}m_{kk} & \cdots & m_{1n} + c_{1n}m_{tt} \\ m_{21} + c_{21}m_{tt} & m_{22} + c_{22}m_{tt} & \cdots & m_{2n} + c_{2n}m_{tt} \\ \vdots & \vdots & \vdots & \vdots \\ m_{n1} + c_{n1}m_{tt} & m_{n2} + c_{n2}m_{tt} & \cdots & m_{kk} + c_{kk}(m_{tt}) \end{bmatrix} = ([m_{\Delta}] + m_{tt}[c]),$$

$$Q_e = \Delta Q_e + m_{kk}c_Q \tag{12}$$

$$[c] = \begin{bmatrix} c_{11} & c_{12} & \cdots & c_{1n} \\ c_{21} & c_{22} & \cdots & c_{2n} \\ \vdots & \vdots & \vdots & \vdots \\ c_{n1} & c_{n2} & \cdots & c_{kk} \end{bmatrix} \tag{13}$$

The linear EVCN that represents the tunable filter with a specified tuning range and reflects the passband variation or the passband tuning behavior is defined. Now, extracting parameters of the EVCN from the general filtering function is of great importance to design the tunable passband with constant BW. The extraction method is derived as follows.

First, the tuning range from  $f_l$  to  $f_h$  is given, and then the mapping frequency can be defined as  $f_d = (f_l + f_h)/2$ . The RL and BW are, respectively, prescribed at RL and ABW. Then, the conventional coupling matrix  $[M]_d$  is extracted at  $f_d$ . Note here that the diagonal elements are all zeros because the resonant frequencies of all resonators are the same (with symmetric distribution) for the simpler case demonstration:

$$[M]_d = \begin{bmatrix} 0 & M_{12} & M_{13} & \cdots & M_{1N} \\ M_{21} & 0 & M_{23} & & M_{2N} \\ M_{31} & M_{32} & \ddots & & \vdots \\ \vdots & & & \ddots & M_{N-1,N} \\ M_{N1} & & & & 0 \end{bmatrix} \tag{14}$$

The coupling matrix response can be mapped to  $f_d$ , scaled by  $ABW/f_l$  and moved to  $f_l$ . Thus, the coupling matrix is expressed as:

$$\begin{cases} [m](m_{tt} = m_{ttl}) = [M]_d \cdot (ABW/f_l) + [W] \cdot m_{ttl} \\ Q_{el} = q_e/(ABW/f_l) \end{cases} \quad (15)$$

$[W]$  is an identity matrix. Similarly, the coupling matrix response can be mapped to  $f_d$ , scaled by  $ABW/f_h$ , and moved to  $f_h$ . Then the coupling matrix is written as:

$$\begin{cases} [m](m_{tt} = m_{tth}) = [M]_d \cdot (ABW/f_h) + [W] \cdot m_{tth} \\ Q_{eh} = q_e/(ABW/f_h) \end{cases} \quad (16)$$

Using linear interpolation, the EVCM can be extracted as:

$$\begin{cases} [m_\Delta]_t = ([m_\Delta] + m_{tt}[c]) \\ Q_e = \Delta Q_e + m_{tt}c_Q \end{cases} \quad (17)$$

where

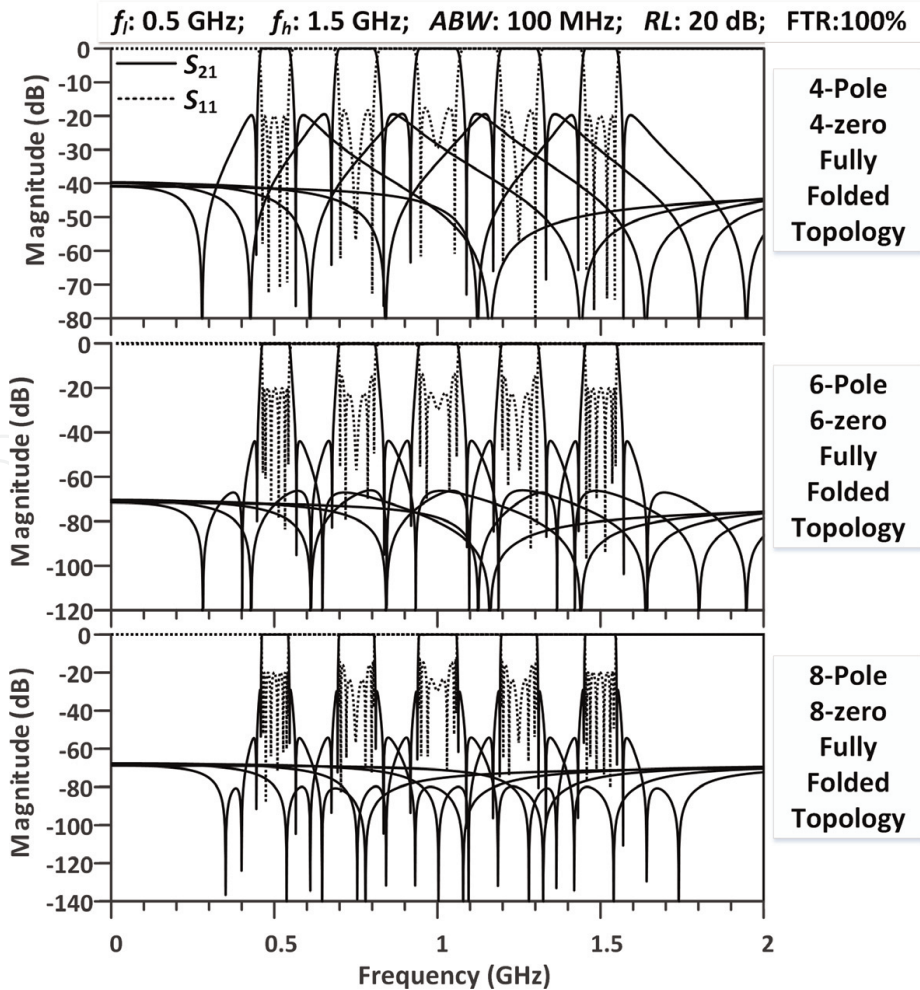


Figure 15. Extracted 100% tunable 4<sup>th</sup>-/6<sup>th</sup>-/8<sup>th</sup>-order responses with constant 100-MHz ABW.

$$\left\{ \begin{array}{l} [m_{\Delta}] = ABW \cdot [M]_d \cdot \left( \frac{(f_h + f_l)}{f_d^2 + f_h f_l} \right) \\ [c] = [M]_d ABW \cdot \frac{f_d (f_l - f_h)}{(f_l f_d^2 - f_h f_d^2 - f_l f_h^2 + f_l^2 f_h)} + [W] \\ \Delta Q_e = \frac{q_e}{ABW} \left( \frac{f_d^2 (f_h + f_l)}{f_d^2 + f_h f_l} \right) \\ c_Q = \frac{q_e}{ABW} \left( - \frac{(f_d f_h f_l)}{f_d^2 + f_h f_l} \right) \end{array} \right. \quad (18)$$

Now the extraction process is completed and the constant-BW tunable filter is synthesized by the EVCN.

For illustration, the 4<sup>th</sup>-/6<sup>th</sup>-/8<sup>th</sup>-order fully canonical folded filters are extracted with 20-dB RL, a 100% frequency tuning range (from 0.5 GHz to 1.5 GHz), and a constant 100 MHz *ABW*. The extracted EVCNs are given as follows:

Four-pole filter:

$$\left\{ \begin{array}{l} [m]_{4-pole} = \begin{cases} m_{12} = 0.09259 + m_{kk} \cdot 0.0463 \\ m_{23} = 0.095338 + m_{kk} \cdot 0.04767 \\ m_{14} = -0.04064 - m_{kk} \cdot 0.0203 \end{cases} \\ Q_{e4-pole} = 11.114465 - m_{kk} \cdot 4.1679, m_{sl} = -5.15e-04 \end{array} \right. \quad (19)$$

Six-pole filter:

$$\left\{ \begin{array}{l} [m]_{6-pole} = \begin{cases} m_{12} = 0.09487 + m_{kk} \cdot 0.04744 \\ m_{23} = 0.066177 + m_{kk} \cdot 0.03309 \\ m_{34} = 0.080465 + m_{kk} \cdot 0.04023 \\ m_{25} = -0.01828 - m_{kk} \cdot 0.0091 \\ m_{16} = 0.00137 + m_{kk} \cdot (6.867e-04) \end{cases} \\ Q_{e6-pole} = 11.5384 - m_{kk} \cdot 4.3269, m_{sl} = -1.5e-05 \end{array} \right. \quad (20)$$

Eight-pole filter:

$$\left\{ \begin{array}{l} [m]_{8-pole} = \begin{cases} m_{12} = 0.09232 + m_{kk} \cdot 0.04616 \\ m_{23} = 0.0657 + m_{kk} \cdot 0.03285 \\ m_{34} = 0.0469 + m_{kk} \cdot 0.02345 \\ m_{45} = 0.09855 + m_{kk} \cdot 0.04927 \\ m_{36} = -0.048 - m_{kk} \cdot 0.02404 \\ m_{27} = 0.009 + m_{kk} \cdot 0.0045 \\ m_{18} = -7.28e-04 - m_{kk} \cdot 3.64e - 04 \end{cases} \\ Q_{e8-pole} = 11.84219 - m_{kk} \cdot 4.4408, m_{sl} = 2.057e - 05 \end{array} \right. \quad (21)$$

Figure 15 presents the calculation responses of three extracted EVCMs. It can be seen that the prescribed responses are tuned from 0.5GHz to 1.5 GHz, and their responses are kept nearly constant. Even though such a wide tuning range and 8<sup>th</sup>-order function are predefined, the maximum estimation error of this synthesis method only affects the RL. When the frequency of the passband is tuned closer to the middle point of the tuning range [ $f_d = (f_h+f_l)/2$ ], the most significant RL deviation will be introduced, which will lead to deterioration of the high-order filter. However, it is still acceptable for the high-order tunable design with a wide FTR (100%).

#### 4. Planar and 3D realizations of the constant-BW tunable filter based on the EVCN synthesis

The synthesis method can be used to extract the EVCN according to the prescribed filter specifications. This section will present the planar and 3D tunable filters to realize the extracted EVCNs practically.

##### 4.1 Planar realization example of the constant-BW tunable filter

The resonator of the planar filter example is shown in Figure 16, and the frequency range design method is given in Figure 17. The resonant frequency is tuned by changing variable capacitor  $C_t$ , and the tuning range can be predefined by  $l_1$ . The capacitor loading position  $l_t$  does not noticeably affect the tuning frequency.

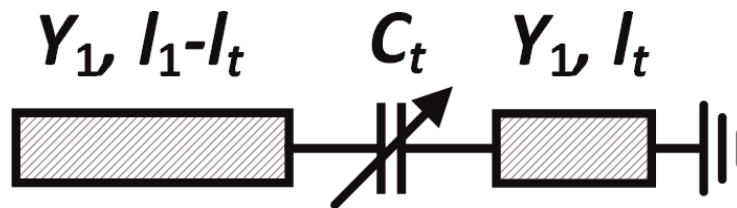


Figure 16. Transmission line model of the synchronously tunable filter resonator.

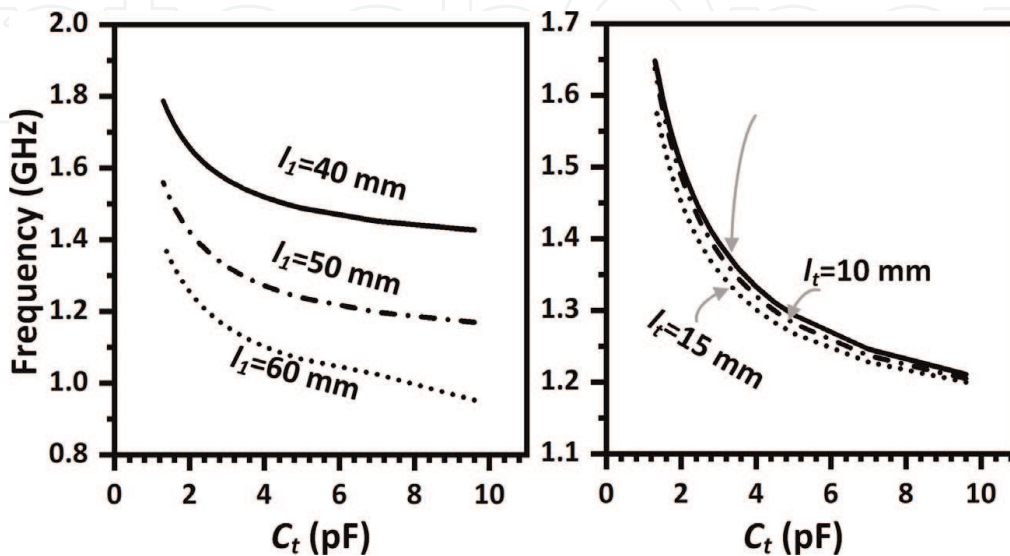


Figure 17. Tunable resonant frequency vs.  $C_t$  with different  $l_1$  or  $l_t$  for (a)  $l_t = 11$  mm (b)  $l_1 = 48.6$  mm.

Figures 18 and 19, respectively, present the electrical coupling (EC) and magnetic coupling (MC) configurations between two planar resonators. Their corresponding coupling coefficient curves extracted from the configurations are shown in Figures 20 and 21. As can be seen, both the slope and position of coupling coefficient curves can be independently controlled with these two coupling configurations. Thus, the coupling elements in the EVCM can be physically realized, and both EC and MC are available.

Two feeding structures, i.e. short-end and open-end feeding structures, can be employed to feed this type of filter, as shown in Figure 22a and b. Figures 23 and 24, respectively, present the extracted external quality factor  $Q_e$  curves for these two configurations. It can be seen that both the slope and position of  $Q_e$  curves are approximately defined by adjusting their physical dimensions independently.

With all filter parts mentioned earlier, two tunable filters using EC and MC as the mainline coupling path to implement the constant BW are demonstrated. Two filters

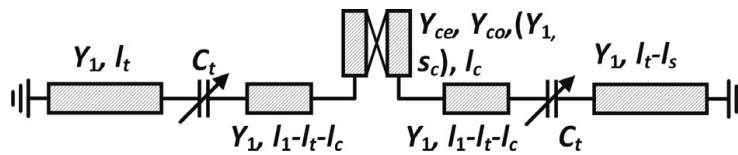


Figure 18.  
EC configuration between resonators.

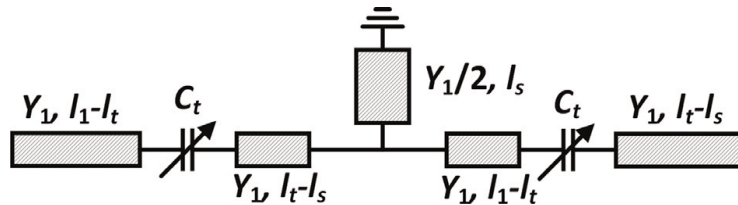


Figure 19.  
MC configuration between resonators.

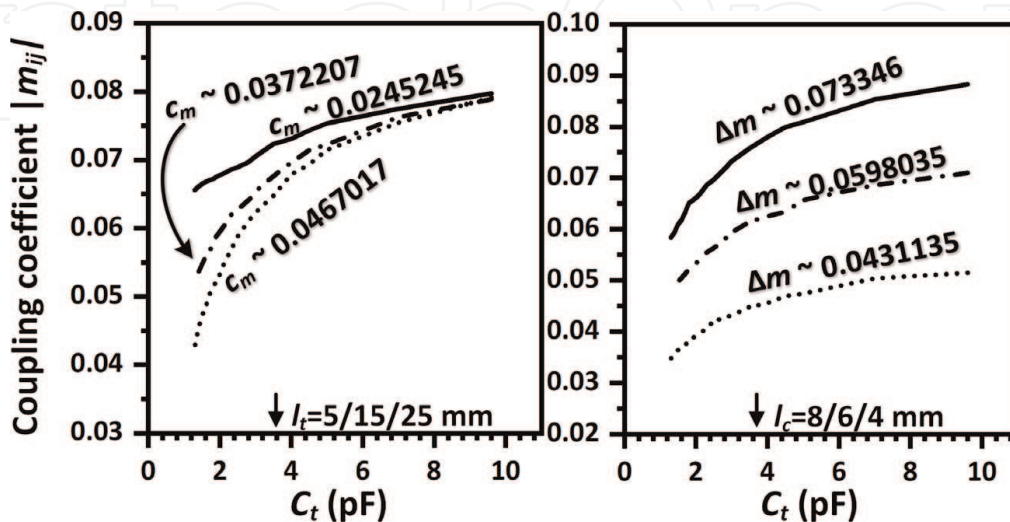
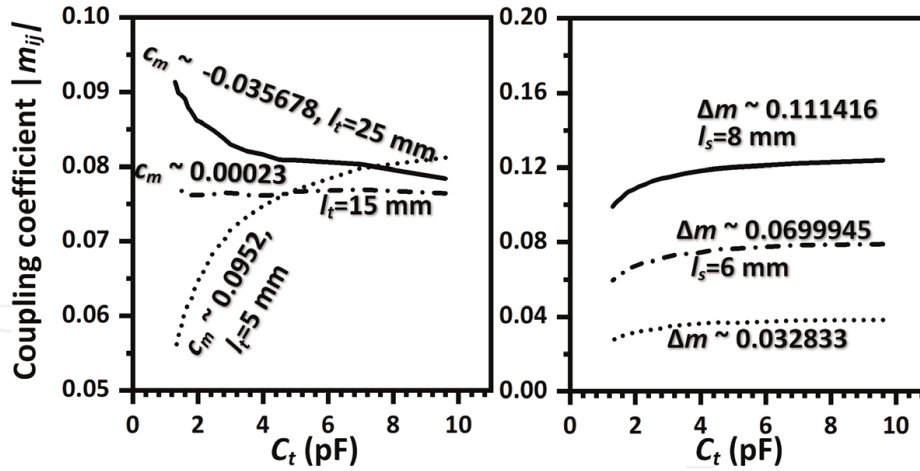
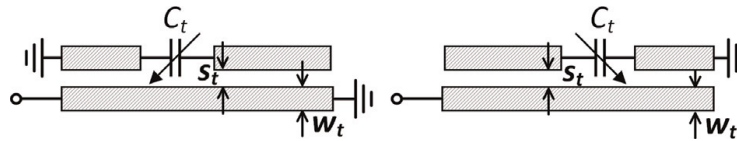


Figure 20.  
Coupling coefficient extracted from the EC configuration (Figure 18) with different  $l_t$  or  $l_c$  when  $s_c = 0.3$  mm for (a)  $l_c = 6.8$  mm (b)  $l_t = 15$  mm.





**Figure 21.** Coupling coefficient extracted from the MC configuration (Figure 19) with different  $l_t$  or  $l_s$  for (a)  $l_s = 5$  mm (b)  $l_t = 8$  mm.



**Figure 22.** (a) S-EF configuration. (b) O-EF configuration.

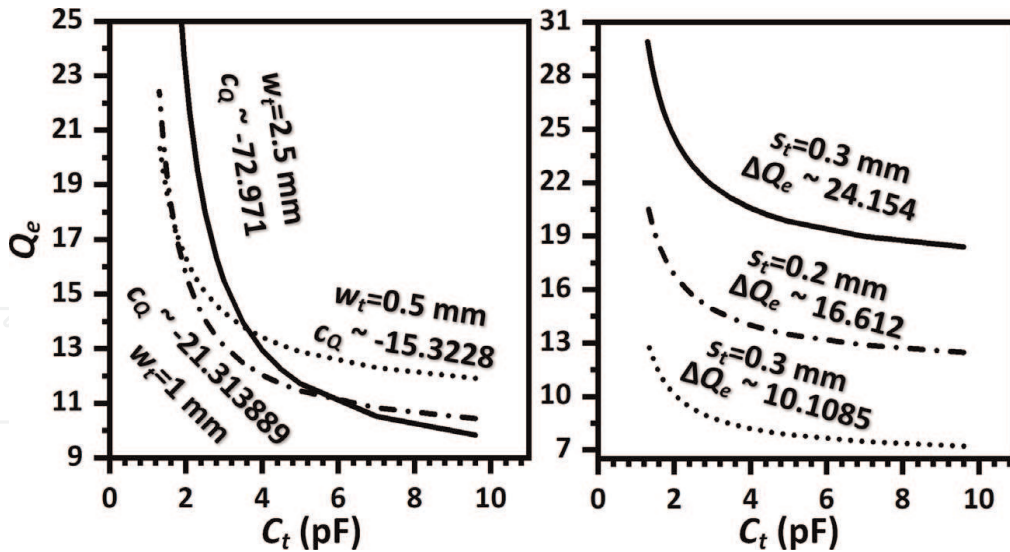


**Figure 23.** External quality factor  $Q_e$  extracted from S-EF configuration (Figure 22a) with different  $w_t$  or  $s_t$  for (a)  $s_t = 0.2$  mm (b)  $w_t = 0.4$  mm.

are the four-pole cascade quartet topology, and their prototypes are the 4<sup>th</sup>-degree General Chebyshev polynomials with 20-RL and 130-MHz ABW. The transmission zeros of two filters are prescribed at  $[-10j, -2j, 2j, 10j]$ . The tuning range of the EC filter is predefined from 1.2 GHz to 1.6 GHz, and the EC filter is from 1.05 GHz to 1.45 GHz. According to the presented synthesis method, two EVCMs can be extracted, which are

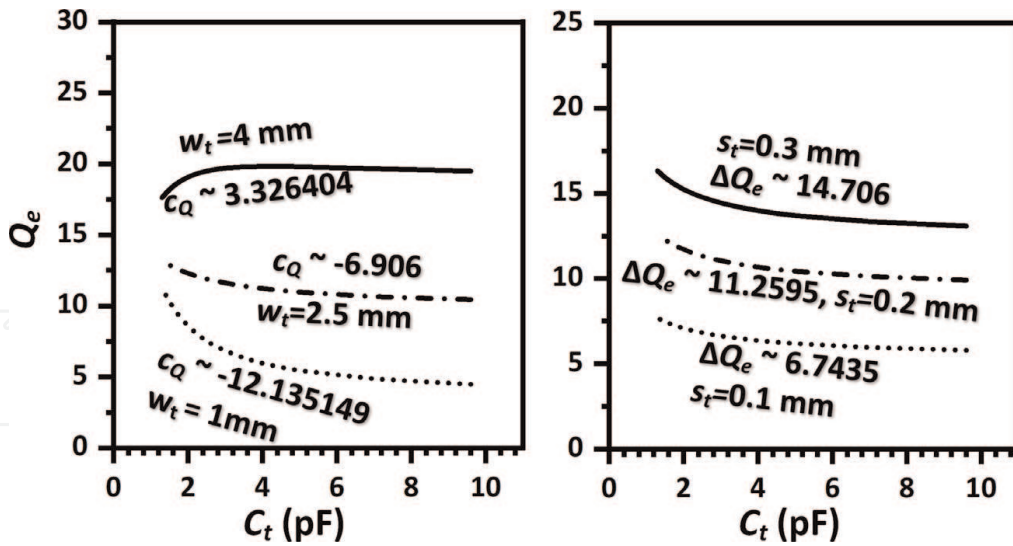


**Figure 24.** External quality factor  $Q_e$  extracted from O-EF configuration (Figure 22b) with different  $w_t$  or  $s_t$  for (a)  $s_t = 0.22$  mm (b)  $w_t = 2.5$  mm.

$$\begin{cases} [m]_{4-pole} = \begin{cases} m_{12} = 0.091646 + m_{kk} \cdot 0.04582 \\ m_{23} = 0.080922 + m_{kk} \cdot 0.04046 \\ m_{14} = -0.0184 - m_{kk} \cdot 0.0092 \end{cases} \\ Q_{e4-pole} = 9.30255 - m_{kk} \cdot 4.5322, m_{sl} = 0.00016 \end{cases} \quad (22)$$

for EC filter and

$$\begin{cases} [m]_{4-pole} = \begin{cases} m_{12} = 0.081612 + m_{kk} \cdot 0.040806 \\ m_{23} = 0.072063 + m_{kk} \cdot 0.036031 \\ m_{14} = -0.01638 - m_{kk} \cdot 0.00819 \end{cases} \\ Q_{e4-pole} = 10.39153 - m_{kk} \cdot 5.0897, m_{sl} = 0.00019 \end{cases} \quad (23)$$

for MC filter. Besides, all filter examples are designed on the Rogers RT/duroid 5880 ( $h = 0.787$  mm,  $\epsilon_r = 2.2$ ,  $\tan\delta = 0.0009$ ) and the variable capacitors are SMV1234 ( $C_t = 1.3$ - $9.6$  pF,  $R_s = 0.8$   $\Omega$ ).

Figures 25 and 26 present the EC and MC filter examples where the cascade quartet configurations are used, thus yielding the prescribed tunable responses with constant BW. The measurement results of the two design examples are shown in Figures 27 and 28. The BW of the two filters is approximately 133 MHz and the tuning ranges are over 27%. Good agreement between simulations and measurements is

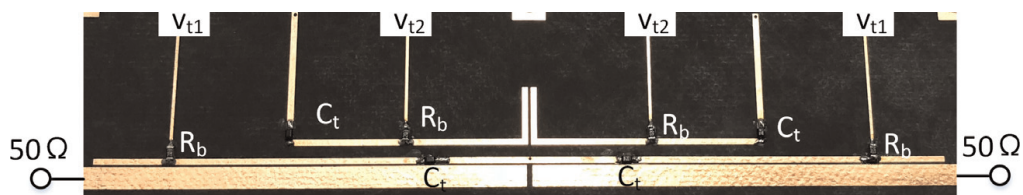


**Figure 25.** EC filter example.

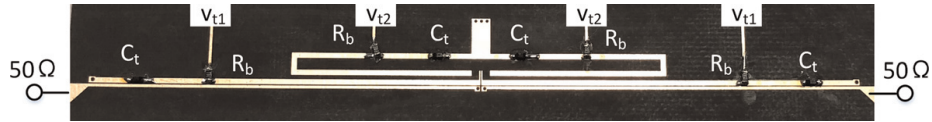


Figure 26. MC filter example.

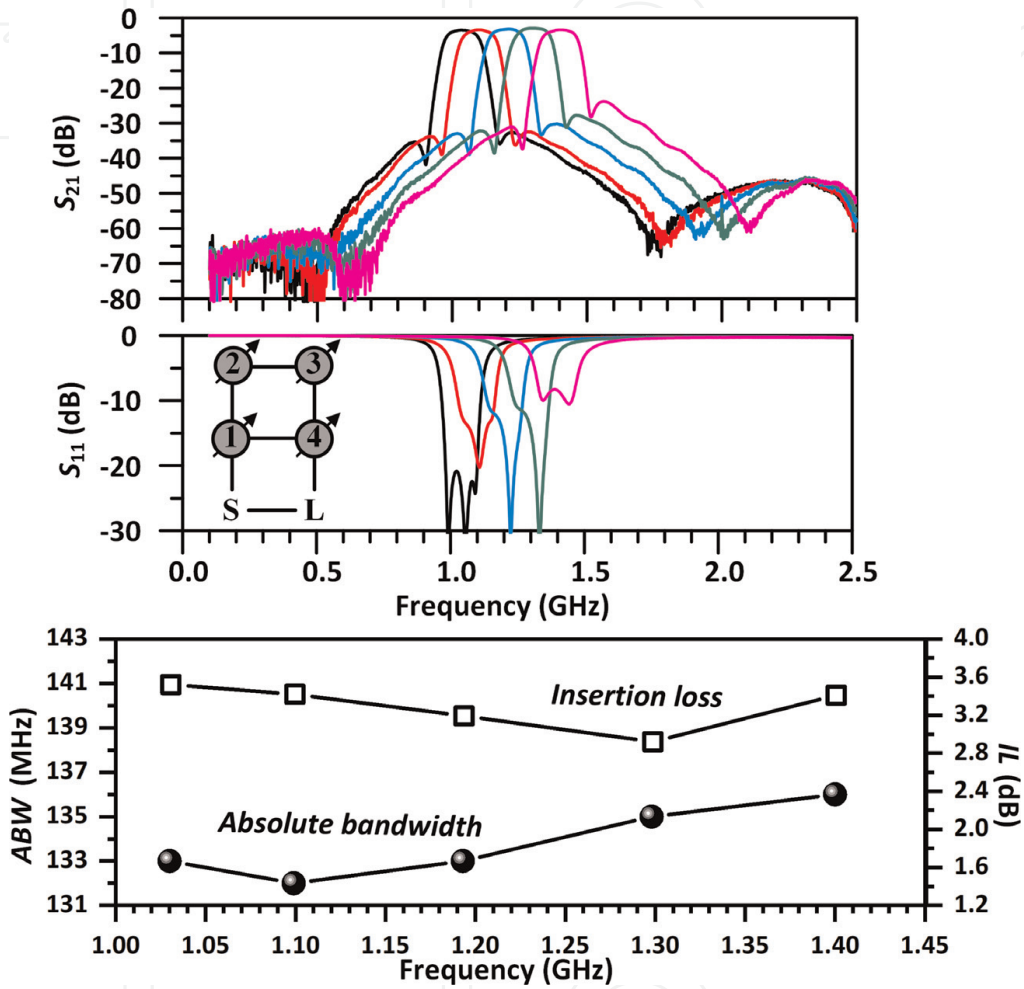


Figure 27. Measurement results of the EC filter example (Figure 25).

achieved, and the design objective is fully implemented. It is noted that the MC filter has a more stable BW because of the more flexible choosing range of coupling and  $Q_e$  curves with the wider adjusting ranges.

#### 4.2 3D realization example of the constant-BW tunable filter

The ceramic monoblock waveguide filter featured a low-cost and competitive  $Q_u$ /size ratio that attracted a great deal of attention for 5G applications [39]. The 3D realization example of the constant-BW tunable filter presented in this section will be based on the ceramic monoblock waveguide structure and the high-Q mechanically tunable mechanism.

Figure 29 present the tunable ceramic monoblock waveguide resonator. It generally contains the fixed block and the movable cylinder. The low-dielectric ( $\epsilon_r = 19.5$ )

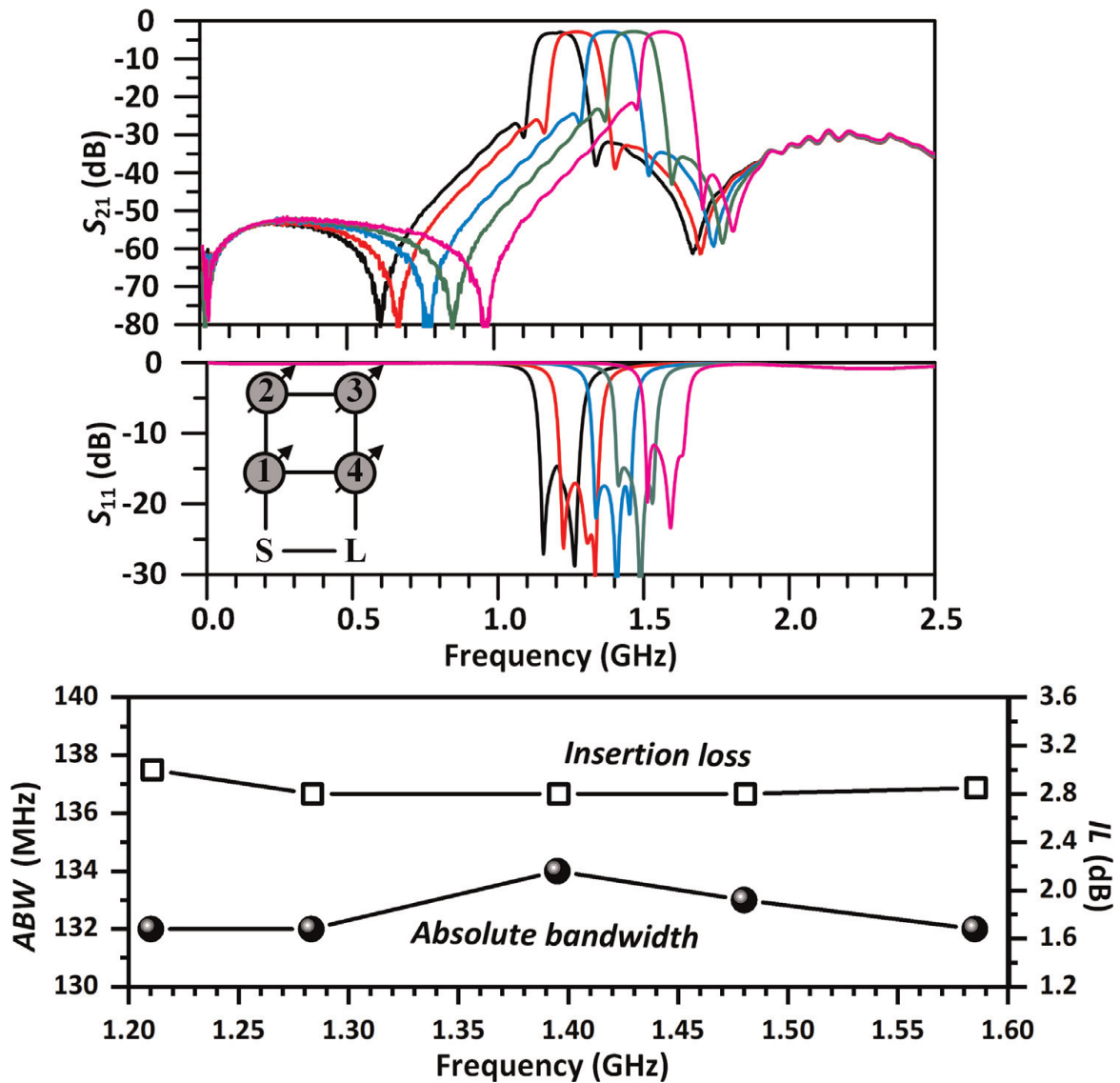


Figure 28. Measurement results of the MC filter example (Figure 26).

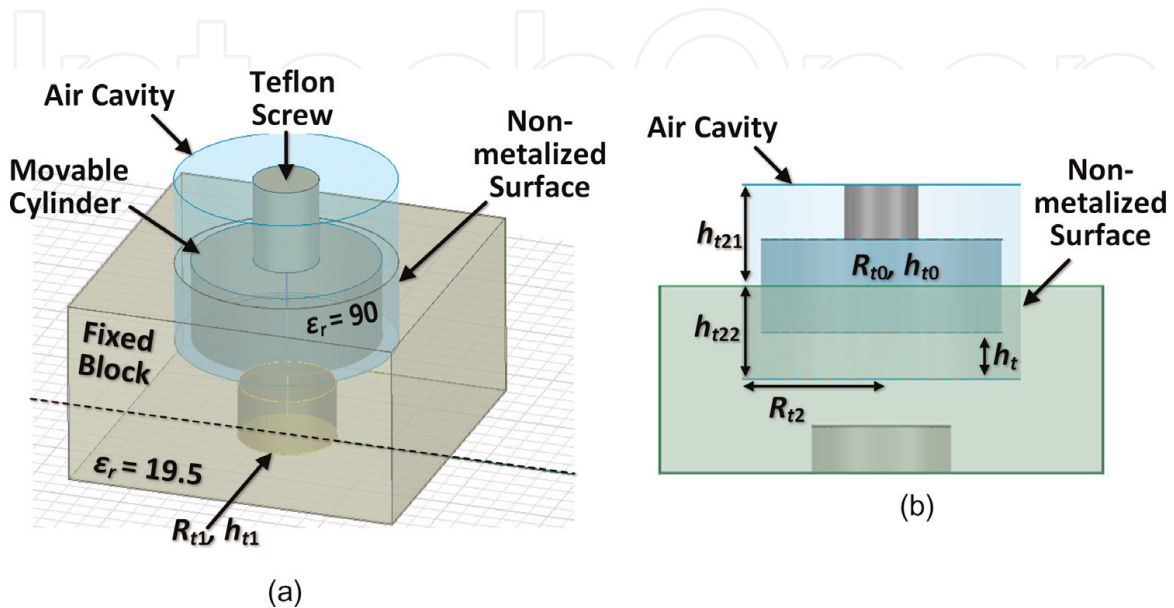
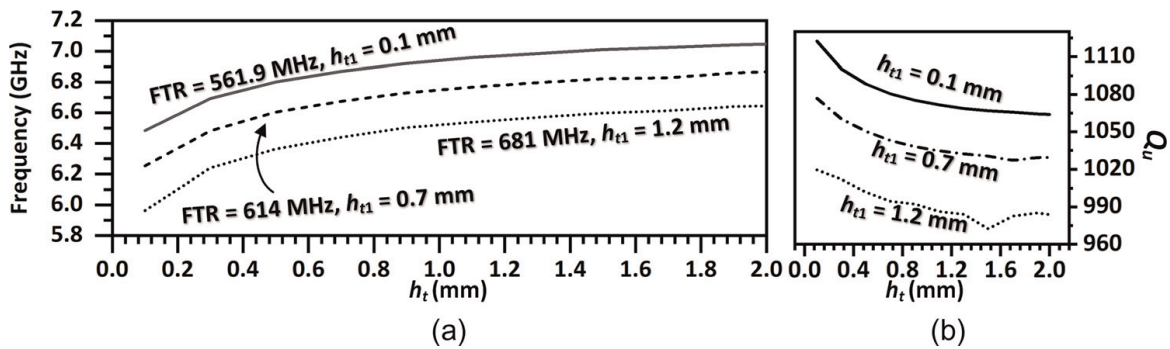


Figure 29. Tunable resonator of ceramic monoblock waveguide filter. (a) 3D model and (b) cross-sectional view.

fixed block is coated with the silver layer except for the big center hole ( $h_{t21}, h_{t22}, R_{t2}$ ). The hole on the bottom ( $h_{t1}, R_{t1}$ ) is metalized. The movable cylinder ( $\epsilon_r = 90$ ) is not coated with the silver layer and can be dragged up and down in the non-metalized hole. The Teflon screw (M0.8) is employed to control the movable cylinder via a driving mechanism. The non-metalized hole with a lid constructs an air cavity to accommodate the movable cylinder. As the ceramic cylinder moves in the air cavity, the resonator's resonant frequency is tuned. **Figure 30** presents the tuning frequency ranges and the  $Q_u$  performance by changing  $h_{t1}$ . As expected, the frequency is tuned by changing the positions of the movable cylinder, and the  $Q_u$  is always kept on a high level. The frequency tuning range can be predefined by  $h_{t1}$ .

The coupling configuration between two resonators is shown in **Figure 31**. The extracted coupling coefficient curves with different key dimensions are presented in **Figure 32**. It is seen that the coupling coefficient curve is controlled by  $h_{m1}$  and  $R_{m1}$ .  $h_{m1}$  and  $R_{m1}$  have more influence in the coupling curve's high-frequency area and low-frequency area, respectively.

The feeding configuration for the tunable ceramic waveguide resonator is given in **Figure 33**, where the resonator is fed by a coplanar waveguide (CPW) line on the bottom of the fixed block. The external  $Q_e$  can be evaluated by the single-end group delay of the fed resonator structure using  $Q_e = 2\pi f_0 \cdot \tau_{11}(f_0)/4$ [20]. **Figure 34** shows the



**Figure 30.** Resonant behavior of the tunable resonator with different  $h_{t1}$ . (a) Resonant frequency tuning ranges and (b) unloaded  $Q_u$  factor performance.

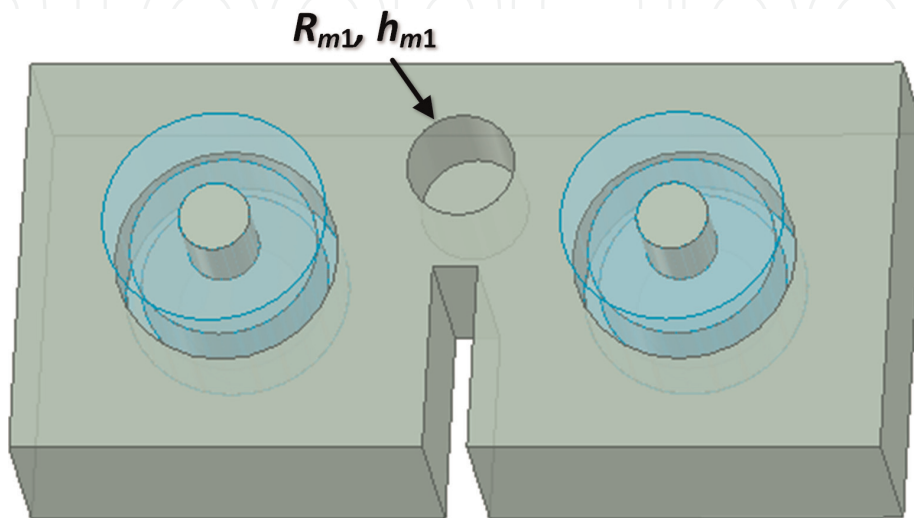


**Figure 31.** Coupling configuration between two resonators.

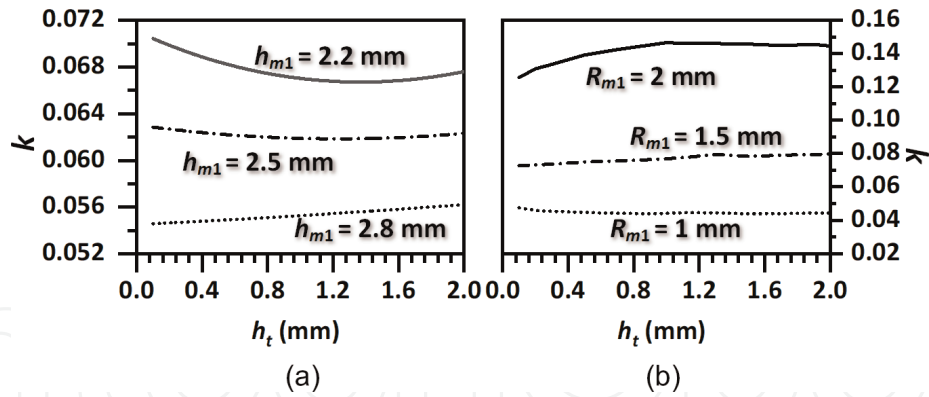


Figure 32. Extracted coupling coefficient curves with different (a)  $h_{m1}$  and (b)  $R_{m1}$ .

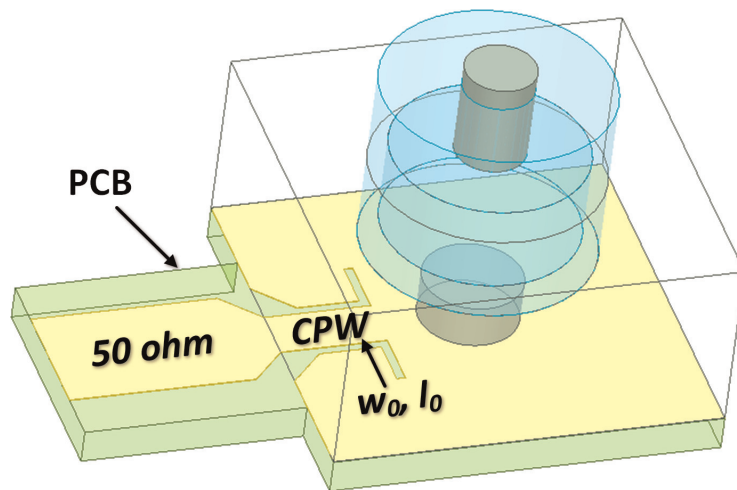


Figure 33. Feeding structures excited using stripline.

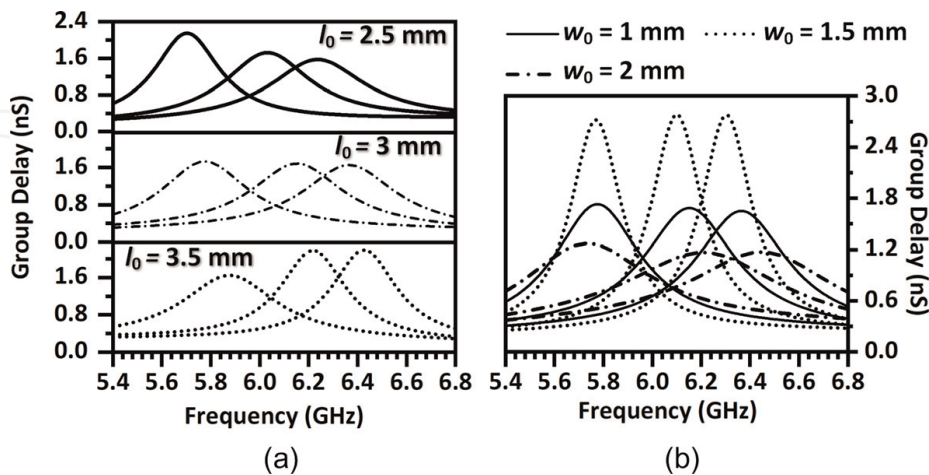


Figure 34. Group delay responses of the feeding structures with different (a)  $l_0$  and (b)  $w_0$ .

extracted group delay. The observation implies that the variation tendency of the  $Q_e$  is controlled by  $l_0$  and the magnitude is controlled by  $w_0$  independently.

With the tunable resonator, coupling structure, and feeding configuration discussed earlier, the ceramic waveguide tunable filter can be constructed. For the demonstration,

the six-degree Chebyshev low-pass prototype with 17-dB return loss and two TZs ( $\pm 1.19511j$ ) is employed to form the two-section cascade-triplet topology. The EVC is extracted for the 5.8–6.2 GHz constant-400-MHz bandwidth filter as:

$$\left\{ \begin{array}{l} m_{s1} = m_{6l} = 0.031m_{kkt} + 0.062 \\ m_{12} = -0.0194m_{kkt} - 0.0388 \\ m_{23} = -0.0134m_{kkt} - 0.0268 \\ m_{34} = -0.0189m_{kkt} - 0.0379 \\ m_{45} = -0.0134m_{kkt} - 0.0268 \\ m_{56} = -0.0194m_{kkt} - 0.0388 \end{array} \right\}, \text{ and } \left\{ \begin{array}{l} m_{13} = -0.0171m_{kkt} - 0.0341 \\ m_{46} = 0.0171m_{kkt} + 0.0341 \\ m_{22} = 1.0247m_{kkt} + 0.0493 \\ m_{33} = 0.9986m_{kkt} - 0.0029 \\ m_{44} = 1.0014m_{kkt} + 0.0029 \\ m_{55} = 0.9753m_{kkt} - 0.0493 \end{array} \right. \quad (24)$$

EM design according to the extracted EVC is carried out, and the optimized filter structure with the manufactured design sample is given in **Figure 35**. The feeding circuit is on Rogers RT/duroid 5880.

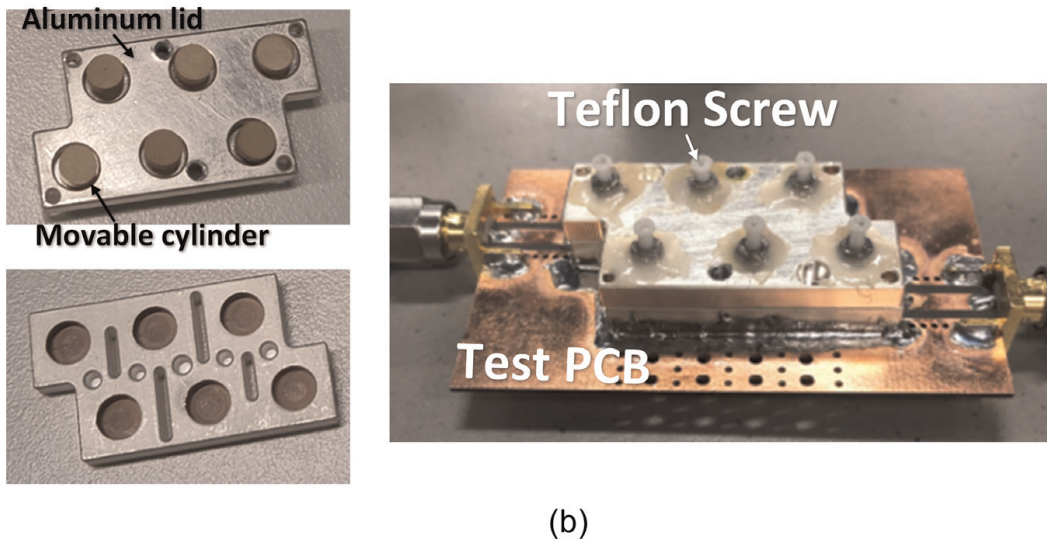
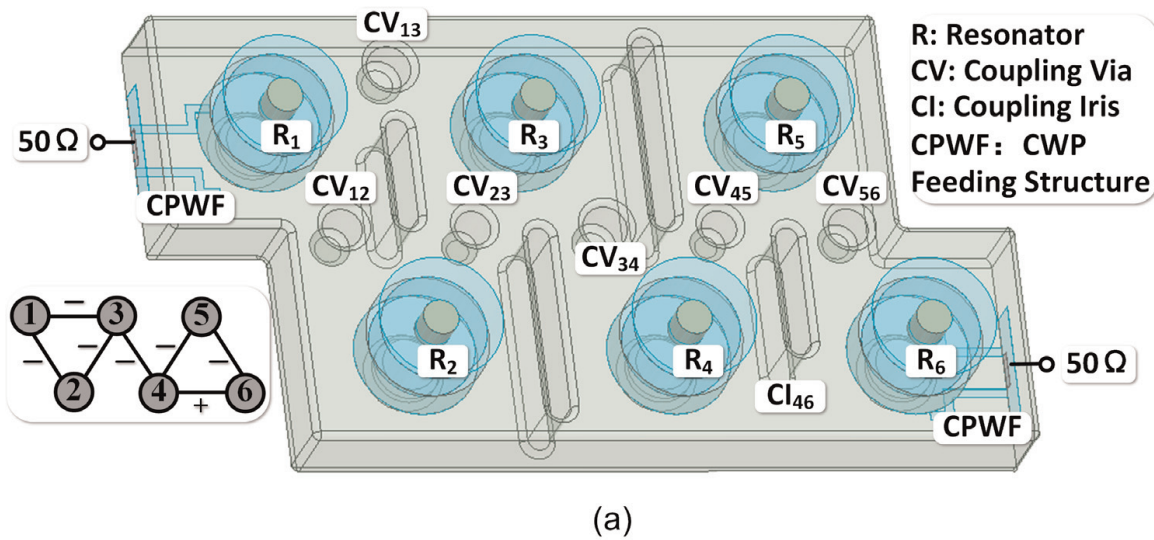


**Figure 35.** Six-pole quasi-elliptic ceramic waveguide filter with constant absolute bandwidth. (a) Filter structure and (b) filter photograph.

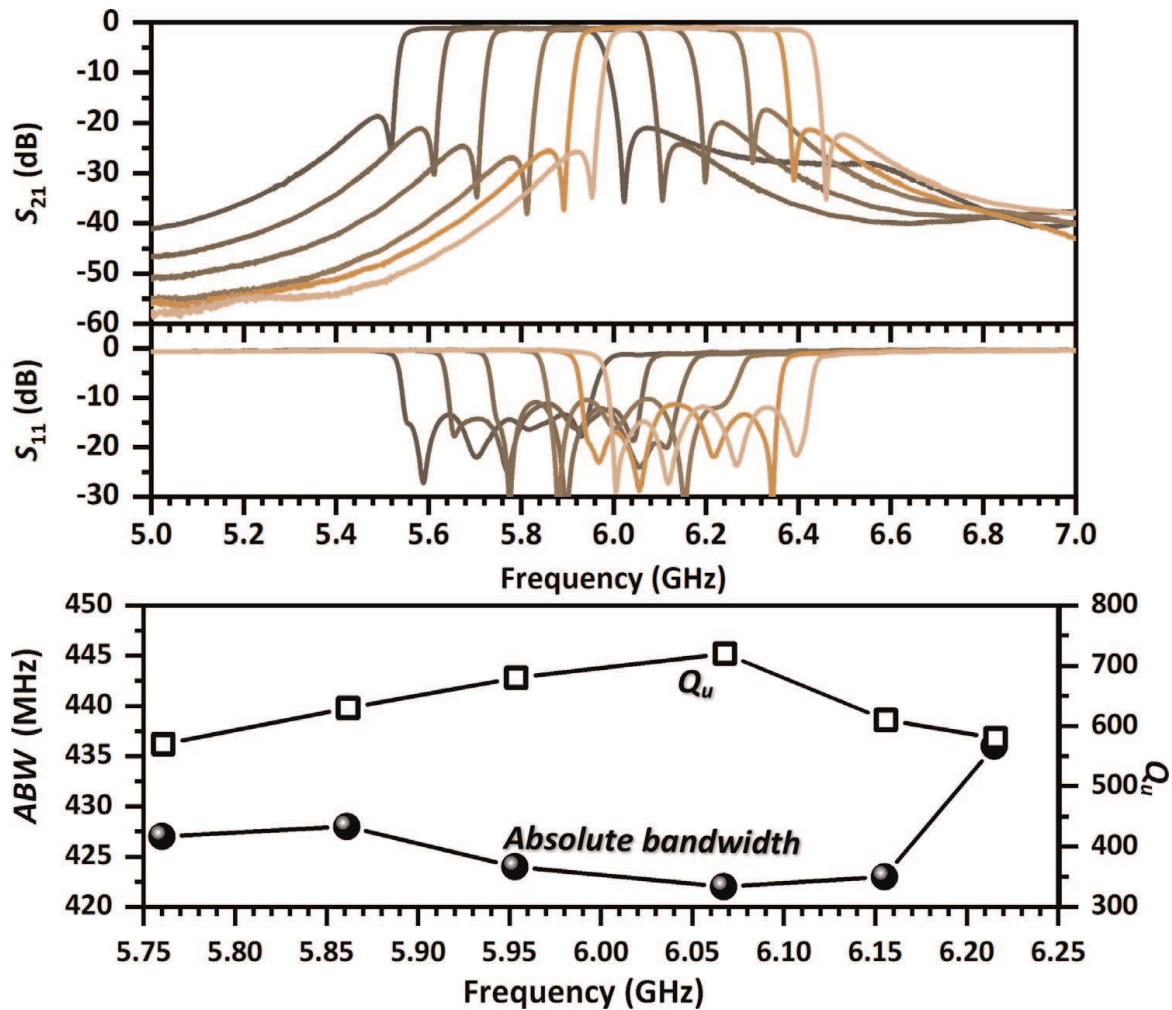


Figure 36.  
 Measurement results of the manufactured design sample.

Figure 36 presents the measured responses of the tunable ceramic waveguide filter. The measured passband moves from 5.76 GHz to 6.22 GHz, but the 3-dB bandwidth maintains  $429 \pm 7$  MHz. The rectangular factor of two skirts is better than 12 dB/20 MHz because of two symmetric transmission zeros. The fitted  $Q_u$  of the tunable filter is kept from 570 to 720.

## 5. Conclusions

EVCN is introduced to represent the tunable filter with its tuning behavior. The relationship between the matrix and physical circuit is established, and this correspondence is investigated in detail. The synthesis approach based on EVCN extraction techniques is presented, and the planar as well as the ceramic waveguide tunable filters are designed according to the approach. The experiment is carried out to confirm the theory.



IntechOpen

IntechOpen

### **Author details**


Di Lu

Southern University of Science and Technology, Shenzhen, China

\*Address all correspondence to: [ludi888abc@hotmail.com](mailto:ludi888abc@hotmail.com)

### **IntechOpen**

---

© 2022 The Author(s). Licensee IntechOpen. This chapter is distributed under the terms of the Creative Commons Attribution License (<http://creativecommons.org/licenses/by/3.0>), which permits unrestricted use, distribution, and reproduction in any medium, provided the original work is properly cited. 

## References

- [1] Liu X. High-Q RF-mems tunable resonators and filters for reconfigurable radio frequency front-ends [Doctor of Philosophy thesis]. Purdue University; 2010
- [2] Aigle M, Hechtfisher G, Hohenester W, et al. A systematic way to YIG-filter-design. In: 2007 European Microwave Conference. Munich, Germany. 2007. pp. 668-671
- [3] Adam JD, Davis LE, Dionne GF, et al. Ferrite devices and materials. IEEE Transactions on Microwave Theory and Techniques. 2002;**50**:721-737
- [4] George LM, Leo Y, Jones EMT. Microwave Filters, Impedance-Matching Networks, and Coupling Structures. Dedham, MA: Artech House; 1980
- [5] Cameron RJ, Kudsia CM, Mansour RR. Microwave Filters for Communication Systems: Fundamentals, Design, and Applications. New York: Wiley-Interscience; 2007
- [6] Laplanche E, Delhote N, Périgaud A, et al. Tunable filtering devices in satellite payloads: A review of recent advanced fabrication technologies and designs of tunable cavity filters and multiplexers using mechanical actuation. IEEE Microwave Magazine. 2020;**21**: 69-83
- [7] Fouladi S, Huang F, Yan WD, et al. High-Q narrowband tunable combline bandpass filters using MEMS capacitor banks and piezomotors. IEEE Transactions on Microwave Theory and Techniques. 2013;**61**:393-402t
- [8] Iskander MA, Nasresfahani M, Mansour RR. A constant-Q tunable combline bandpass filter using angular tuning technique. 2014 44th European Microwave Conference. 2014. p. 1103–1106
- [9] Mansour BG. A tunable quarter-wavelength coaxial filter with constant absolute bandwidth using a single tuning element. IEEE Microwave and Wireless Components Letters. 2021;**31**:658-661
- [10] Basavarajappa G, Mansour RR. Design methodology of a high- $Q$  tunable coaxial filter and diplexer. IEEE Transactions on Microwave Theory and Techniques. 2019;**67**:5005-5015
- [11] Yassini B, Yu M, Keats B. A ka -band fully tunable cavity filter. IEEE Transactions on Microwave Theory and Techniques. 2012;**60**:4002-4012
- [12] Arnold C, Parlebas J, Zwick T. Reconfigurable waveguide filter with variable bandwidth and center frequency. IEEE Transactions on Microwave Theory and Techniques. 2014;**62**:1663-1670
- [13] Ossorio J, Vague J, Boria VE, et al. Exploring the tuning range of channel filters for satellite applications using electromagnetic-based computer aided design tools. IEEE Transactions on Microwave Theory and Techniques. 2018;**66**:717-725
- [14] Gowrish B, Mansour RR. A dual-mode frequency reconfigurable waveguide filter with a constant frequency spacing between transmission zeros. In: 2020 IEEE/MTT-S International Microwave Symposium (IMS). 2020. pp. 811-814
- [15] Basavarajappa G, Mansour RR. Design methodology of a tunable waveguide filter with a constant absolute bandwidth using a single tuning element. IEEE Transactions on Microwave Theory and Techniques. 2018;**66**:5632-5639

- [16] Wang C, Blair WD. Tunable high-Q dielectric loaded resonator and filter. In: Proceedings RAWCON 2002 2002 IEEE Radio and Wireless Conference (Cat No02EX573). 2002. pp. 249-252
- [17] Pance K, Rochford G. Multiple band and multiple frequency dielectric resonators tunable filters for base stations. In: 2008 38th European Microwave Conference. 2008. pp. 488-491
- [18] Shen T, Zaki KA, Wang C. Tunable dielectric resonators with dielectric tuning disks. *IEEE Transactions on Microwave Theory and Techniques*. 2000;**48**:2439-2445
- [19] Hunter IC, Rhodes JD. Electronically tunable microwave bandstop filters. *IEEE Transactions on Microwave Theory and Techniques*. 1982;**30**:1361-1367
- [20] Hong J-SG, Lancaster MJ. *Microstrip Filters for RF/Microwave Applications*. NJ, USA: Wiley; 2004
- [21] Guyette A. Controlled agility: Frequency-agile planar filters with advanced features. *IEEE Microwave Magazine*. 2014;**15**:32-42
- [22] Islam H, Das S, Bose T, et al. Diode based reconfigurable microwave filters for cognitive radio applications: A review. *IEEE Access*. 2020;**8**: 185429-185444
- [23] Lu D, Tang X, Barker NS, et al. Synthesis-applied highly selective tunable dual-mode BPF with element-variable coupling matrix. *IEEE Transactions on Microwave Theory and Techniques*. 2018;**66**: 1804-1816
- [24] Rebeiz G, Entesari K, Reines I, et al. Tuning in to RF MEMS. *IEEE Microwave Magazine*. 2009;**10**:55-72
- [25] Tombak A, Maria J-P, Ayguavives FT, et al. Voltage-controlled RF filters employing thin-film barium-strontium-titanate tunable capacitors. *IEEE Transactions on Microwave Theory and Techniques*. 2003;**51**:462-467
- [26] Entesari K, Saghati AP, Sekar V, et al. Tunable SIW structures: Antennas, VCOs, and filters. *IEEE Microwave Magazine*. 2015;**16**:34-54
- [27] Park S-J, Reines I, Patel C, et al. High-Q RF-MEMS 4–6-GHz tunable evanescent-mode cavity filter. *IEEE Transactions on Microwave Theory and Techniques*. 2010;**58**:381-389
- [28] Kang Q, Shamsaifar K. Electronically Tunable Block Filter with Tunable Transmission Zeros. Google Patents; 2004
- [29] Anand A, Small J, Peroulis D, et al. Theory and design of octave tunable filters with lumped tuning elements. *IEEE Transactions on Microwave Theory and Techniques*. 2013;**61**:4353-4364
- [30] Xu J, Yang L, Yang Y, et al. High-Q-factor tunable bandpass filter with constant absolute bandwidth and wide tuning range based on coaxial resonators. *IEEE Transactions on Microwave Theory and Techniques*. 2019;**67**:4186-4195
- [31] Yang Z, Psychogiou D, Peroulis D. Design and optimization of tunable silicon-integrated evanescent-mode bandpass filters. *IEEE Transactions on Microwave Theory and Techniques*. 2018;**66**:1790-1803
- [32] Mansour RR. High-Q tunable dielectric resonator filters. *IEEE Microwave Magazine*. 2009;**10**:84-98
- [33] Xu J, Zhang XY, Li H, et al. Narrowband single-pole double-throw filtering switch based on dielectric

resonator. *IEEE Microwave and Wireless Components Letters*. 2018;**28**:594-596

[34] Pelliccia L, Cacciamani F, Farinelli P, et al. High-Q tunable waveguide filters using ohmic RF MEMS switches. *IEEE Transactions on Microwave Theory and Techniques*. 2015;**63**:3381-3390

[35] Park SJ, Rebeiz GM. Low-loss two-pole tunable filters with three different predefined bandwidth characteristics. *IEEE Transactions on Microwave Theory and Techniques*. 2008;**56**:1137-1148

[36] Lu D, Tang X, Barker NS, et al. Single-band and switchable dual-/single-band tunable BPFs with predefined tuning range, bandwidth, and selectivity. *IEEE Transactions on Microwave Theory and Techniques*. 2017;**66**:1215-1227

[37] Lu D, Yu M, Barker NS, et al. Advanced synthesis of wide-tuning-range frequency-adaptive bandpass filter with constant absolute bandwidth. *IEEE Transactions on Microwave Theory and Techniques*. 2019;**67**:4362-4375

[38] Amari S. Synthesis of cross-coupled resonator filters using an analytical gradient-based optimization technique. *IEEE Transactions on Microwave Theory and Techniques*. 2000;**48**:1559-1564

[39] Chen Y, Zhang Y, Wu K-L. A dual-mode monoblock dielectric bandpass filter using dissimilar fundamental modes. *IEEE Transactions on Microwave Theory and Techniques*. 2021;**69**:3811-3819